JTTEE5 4:41-49
©ASM International

Modeling of Particles Impacting on a Rigid Substrate under Plasma Spraying Conditions

M. Bertagnolli, M. Marchese, and G. Jacucci

Finite-element methods have been applied for the spreading process of a ceramic liquid droplet impacting on a flat cold surface under plasma spraying conditions. The goals of the present investigation are to predict the geometrical form of the splat as a function of process parameters, such as initial temperature and velocity, and to follow the thermal field developing in the droplet up to solidification. A nonlinear finite-element procedure has been extended to model the complex physical phenomena involved in the impact process. The dynamic motion of the viscous melt in the drops as constrained by elastic surface tensions and in interaction with the developing contact with the target has been coupled to transient thermal phenomena to account for the solidification of the material. A model is used to study the impact of spherical particles of liquid ceramic of given temperature and velocity on a flat, cool rigid surface. The deformation of the splat geometry as well as the evolution of the thermal field within the splat are followed up to the final state and require adaptive discretization techniques. The proposed model can be used to correlate flattening degrees with the initial process parameters.

1. Introduction

INTHE thermal spray process, a coating layer is formed by the impingement of small molten particles on the substrate. In plasma spraying, a plasma torch is used to melt the particles of the coating material at very high temperature (~20,000 K). The manufacturing process has been described in detail elsewhere (e.g., Ref 1). Coating quality is dependent on a large number of parameters, such as the design and power of the torch, its position relative to the substrate, the type of powder used and how it is introduced into the plasma, and the nature and preparation of the substrate. Traditionally, these parameters have been optimized empirically.

In recent years, much progress has been made in understanding the physics of plasma spraying, particularly the physics of the plasma and the plasma/particle interactions (e.g., Ref 2, 3). A number of investigators (Ref 4, 5) have studied the microstructures of the resulting coatings. The objective of such studies is to understand how the properties of coatings correlate with the process parameters used to obtain them. The present article addresses a fundamental process that influences the final properties of a coating: namely, the heat transfer and fluid flow phenomena associated with the impingement, spreading, and solidification of liquid droplets on solid cool surfaces.

In the plasma spray process, ceramic or metallic powder is fed into a high-temperature, high-velocity arc plasma, where the powder particles melt as they are propelled toward a substrate. The molten material then splats onto the substrate to build up the desired coating. A simulation of a typical single-impact event is shown in Fig. 1. The final microstructure of plasma-sprayed coatings is a result of, and depends on, the details of the spraying process. It is determined by, among other parameters, the velocity, temperature, size distribution, and percentage of molten particles as well as the conditions of spreading and solidification of the impacting particles.

The problem of investigating the in-flight and impact behavior of the melted particles is presently tackled at different levels. Data on heat transfer, fluid flow, and solidification processes can be collected using laser techniques (Ref 6-8), high-speed photography (Ref 9), or videography (Ref 10). However, such information is difficult to obtain and is only available in an extensive form for a limited number of case studies. On the other hand, it is possible to construct theoretical and numerical models to investigate impact processes. Such models, once validated experimentally, can be used to interpret transient behaviors and to extend experimental knowledge to different parameter space re-

Keywords: finite-element method, fluid flow and heat transfer, modeling, particle impact and splat geometry

M. Bertagnolli, M. Marchese, and **G. Jacucci,** University of Trento, Laboratory of Computer Science Engineering, I-38068 Roverto (TN), Italy.

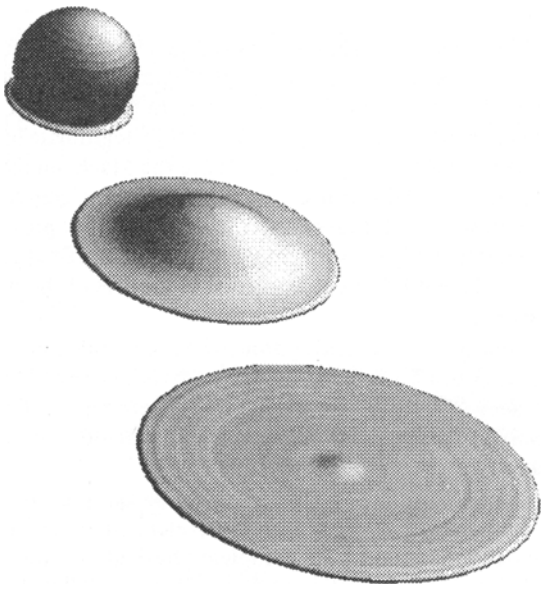

Fig. 1 Evolution of a simulated impact event at 0.05, 0.25, and 0.50 μs for a particle with an initial diameter of 20 μm and a final diameter of approximately 60 μm

gions. Moreover, the output of such experimental and modeling studies is the foundation of discrete models for the spray deposition process (Ref 11, 12). These models can ultimately link single-particle behavior to final coating microstructure and thus to its thermal and mechanical properties.

Madejski (Ref 13) investigated the impingement and solidification of liquid droplets both theoretically and numerically. He made four main assumptions: (1) that the kinetic energy of the particle goes into viscous dissipation and changes in surface tension due to the change of shape, (2) that the particle forms a thin disk, (3) that heat flow is everywhere normal to the surface, and (4) that the simplest velocity distribution satisfies the continuity equation. The model predicts asymptotic values for the flattening degree, ξ (i.e., the ratio of the final disk diameter, D, to that of the original particle, d), of the impacting particles for different cases (degree of solidification, Reynolds number, and Weber number). If it is further assumed that solidification can be ignored, a simple equation for the flattening degree, ξ, can be obtained:

$$\frac{3\xi^2}{W} + \frac{1}{R}\left(\frac{\xi}{1.2941}\right)^5 = 1 \qquad \text{(Eq 1)}$$

provided that the Reynolds number, R, is greater than 100; W is the Weber number. McPherson (Ref 5) has pointed out that for plasma spraying the term $3\xi^2/W$ is negligible. Thus,

$$\xi = \frac{D}{d} = 1.2941\, R^{0.2} = 1.2941 \left(\frac{\rho V d}{\eta}\right)^{0.2} \qquad \text{(Eq 2)}$$

where ρ, V, and η, respectively, are the density, velocity, and viscosity of the particle. For Reynolds numbers below 100, R should be replaced by $R + 0.9517$. This formula has been investigated both experimentally and numerically; results indicate that it tends to overestimate the measured final diameter (Ref 10, 14-17).

A different approach has been developed by Houben (Ref 17, 18) using shock theory, and the morphological characteristics of the final splat shape have been deduced. In this regard it is not clear whether a shock-wave approach is fully legitimate in treating impacts in thermal spraying because the Mach numbers involved are low (0.05 or less), as pointed out by Trapaga and Szekely (Ref 14). Moreover, the approach does not provide an explicit relationship between initial conditions and final geometry—the relevant information needed in models of the deposition process.

A completely numerical approach has been followed by Trapaga et al. (Ref 10, 14) that considers both fluid flow and thermal phenomena. The fluid flow and thermal governing equations are then solved within a finite-difference formulation and implementation.

This article presents a similar model based on a finite-element formulation. A nonlinear finite-element procedure has been extended to model the complete physical phenomena involved. The dynamic motion of the viscous melt in the drops, as constrained by elastic surface tension in interaction with the developing contact with the substrate, is ultimately coupled to transient thermal phenomena. Friction and thermal phenomena, accounting for the solidification of the material, are easily implemented in the finite-element approach.

A brief description of the mathematical and numerical formulation of the problem is presented in Section 2. A more detailed description can be found in Bertagnolli et al. (Ref 19). Section 3 discusses the relevant input parameters and boundary conditions of the model. Results for complete simulations of impact processes and sensitivity studies on the variation of process parameters are reported in detail in Section 4. Use of the proposed model in correlating flattening degrees with the initial process parameters is addressed.

2. Numerical Formulation

2.1 *Impact Motion*

For a numerical analysis of the impact problem, the impinging particle is represented by a finite-element mesh and the material is described as a viscous isochoric medium. The equations of motion for the discretized system in the matrix form can be written, following Argyris et al. (Ref 20) as:

$$\mathbf{MV} + \mathbf{N}[\mathbf{V} - \mathbf{W}] + \mathbf{S} = \mathbf{R} \qquad \text{(Eq 3)}$$

where $\mathbf{M}$ denotes the mass matrix of the system and $\mathbf{N}$ the convective matrix. The vector array, $\mathbf{W}$, comprises the velocities of the nodal points, which can be moved independently of the material particles (of velocity $\mathbf{V}$) temporarily occupying the same locations. Note that the convective term vanishes in a Lagrangean description of the problem in which the reference system moves together with the material ($\mathbf{W} \equiv \mathbf{V}$). The vector $\mathbf{S}$ collects the resultants of the internal stresses at the mesh nodal points, the vector $\mathbf{R}$ the discretized external forces. The applied forces may depend on time and on the actual geometry of the deforming solid.

In particular, for the viscous isochoric medium considered here, the deviatoric part of the element stress is related to the rate of deformation by the viscosity coefficient μ:

$$\sigma_D = 2\mu\delta_D \qquad \text{(Eq 4)}$$

Also, a relaxed isochoric condition is used that relates the hydrostatic stress to a negligible volumetric rate of deformation:

$$\sigma_H = 3\bar{\kappa}\delta_V \qquad \text{(Eq 5)}$$

via the numerical penalty factor $\bar{\kappa}$.

Therefore, the total element stresses, σ, in the viscous solid appear as a function of the velocities of the nodal points in the finite-element mesh collected in the vector array $\mathbf{V}$. This dependence transfers to the stress resultant $\mathbf{S}$ in the equation of motion (Eq 3) and can be indicated as:

$$\mathbf{S} = \bar{\mathbf{D}}\mathbf{V} \qquad \text{(Eq 6)}$$

where $\bar{\mathbf{D}}$ represents the viscosity matrix of the discretized system in terms of the above penalty approach to the isochoric condition.

Returning to the finite-element equation of motion (Eq 3), a fully algebraic equation can be obtained by linking velocity and

acceleration via an approximate integration within a time increment of $\tau = {}^{b}t - {}^{a}t$. The following implicit approximation scheme is based on the acceleration ${}^{b}\dot{\mathbf{V}}$ at the end of the time increment under consideration. It furnishes the velocity

$${}^{b}\mathbf{V} = {}^{a}\mathbf{V} + \tau[c_1\,{}^{a}\dot{\mathbf{V}} + c_2\,{}^{b}\dot{\mathbf{V}}] \qquad \text{(Eq 7)}$$

Also, the nodal point positions, collected in the vector array $\mathbf{X}$,

$${}^{b}\mathbf{X} = {}^{a}\mathbf{X} + \tau\,{}^{a}\mathbf{V} + \tau^2[c_3\,{}^{a}\dot{\mathbf{V}} + c_4\,{}^{b}\dot{\mathbf{V}}] \qquad \text{(Eq 8)}$$

at time instant ${}^{b}t$ at the end of the increment are necessary to obtain the geometry of the discretization mesh if this is chosen to follow the motion of the material. The parameters c_1, c_2, c_3, and c_4 in Eq 7 and 8 control the numerical performance of the integration procedure and may be adapted to particular time-stepping schemes known in the literature.

The system (Eq 3) which may be nonlinear in the velocity is solved for $\mathbf{V} = {}^{b}\mathbf{V}$ at time instant $t = {}^{b}t$ via the recurrence formula:

$$\mathbf{V}_{i+1} = \mathbf{V}_i + \mathbf{H}^{M}_i[\mathbf{R} - \mathbf{S} - \mathbf{N}[\mathbf{V} - \mathbf{W}] - \mathbf{M}\dot{\mathbf{V}}]_i \qquad \text{(Eq 9)}$$

and furnishes the result of iteration $i + 1$ using the data obtained in the ith iteration cycle. The best choice for the iteration matrix $\mathbf{H}^{M}$ is based on the inverse of the gradient of the residuum within the brackets in Eq 9 with respect to $\mathbf{V}$. For convenience, the latter is approximated by:

$$\mathbf{G} \leftarrow -\left[\bar{\mathbf{D}} + \frac{1}{\tau b}\mathbf{M}\right] \qquad \text{(Eq 10)}$$

which considers the inertia term and accounts for a linear dependence of the stress resultants on velocity; in this way, the nonsymmetric contribution from the convective term is avoided, as is a possible dependence of the applied forces on kinematics.

When points on the surface of the medium contact the target, contact forces $\mathbf{F}_n$ normal to the surface and friction forces $\mathbf{F}_t$ tangential to the surface are accounted for via (Ref 21):

$$\mathbf{F}_n = -k_n v_n \qquad \text{(Eq 11)}$$

and

$$\mathbf{F}_t = -k_t v_t \qquad \text{(Eq 12)}$$

Because the material velocity v_n normal to the surface of the target must be suppressed upon contact, $k_n \to \infty$ represents a penalty factor associated with a relaxed contact condition. The factor

$$k_t = |\mathbf{F}_t| / |v_t| \le k_{max} \qquad \text{(Eq 13)}$$

in the above kinematic formulation of the friction force opposed to the tangential velocity, v_t, does not restrict the friction law for $|\mathbf{F}_t|$. The limitation by k_{max} corresponds to a penalty approach to the condition of striking.

The contact reactions act on the medium in addition to the applied forces. The complete kinematic description of the contact forces by Eq 11 and 12, in conformity with the viscous nature of the deformation problem, suggests a modification of the stress resultants in the system by:

$$\mathbf{S} - \mathbf{F} = [\bar{\mathbf{D}} + \mathbf{K}]\mathbf{V} \qquad \text{(Eq 14)}$$

and accordingly of the system matrix in Eq 10.

In Eq 14, $\mathbf{K}$ denotes a diagonal hypermatrix accounting for the joint action of $\mathbf{F}_n$ and $\mathbf{F}_t$ at the nodal points currently in contact with the target. Therefore, the structure of the system matrix is not affected by the variation of the boundary conditions during the course of the impact.

2.2 *Thermal Phenomena*

During impact, intense thermal phenomena occur that significantly influence the formation of the microstructure and the deformation of the impacting liquid through a temperature-dependent viscosity coefficient and the process of solidification. The temperature field is governed by the energy balance, which in the finite-element formulation of the thermal problem can be expressed by a matrix equation following Argyris et al. (Ref 20):

$$\mathbf{C}\dot{\mathbf{T}} + \mathbf{K}\mathbf{T} + \mathbf{L}\mathbf{T} = \dot{\mathbf{Q}} \qquad \text{(Eq 15)}$$

where $\mathbf{T}$ and $\dot{\mathbf{T}}$ are vector arrays comprising the temperatures and their time rates at the nodes of the finite-element mesh, and $\dot{Q}$ represents the heat fluxes at the nodal points. The latter reflect the rate of mechanical dissipation and part of the heat transfer through the surface. The matrices $\mathbf{C}$, $\mathbf{K}$, and $\mathbf{L}$ represent the heat capacity, convection, and conductivity of the system, respectively. The convection matrix $\mathbf{K}$ refers to the expression for the time rate of the particle temperature and vanishes in a Lagrangean description of the problem in which the reference system moves together with the material ($\mathbf{W} \equiv \mathbf{V}$). The conductivity matrix $\mathbf{L}$ comprises, in addition, that part of the heat transfer through the surface which depends on the actual temperature. To account for solidification, the associated latent heat effect is modeled by a suitable modification of the specific heat capacity in the matrix $\mathbf{C}$ within the temperature interval specifying the change from the liquid to the solid phase.

A fully algebraic equation for the thermal problem is obtained by linking the temperature and its time rate within a time increment $\tau = {}^{b}t - {}^{a}t$ by the approximation scheme:

$${}^{b}\mathbf{T} = {}^{a}\mathbf{T} + (1 - \zeta)\tau\,{}^{a}\dot{\mathbf{T}} + \zeta\tau\,{}^{b}\dot{\mathbf{T}} \qquad \text{(Eq 16)}$$

where

$$0 \le \zeta \le 1 \qquad \text{(Eq 17)}$$

is a collocation parameter. At a fixed state of motion, the solution of the system (Eq 15) in conjunction with Eq 16 may then be performed for the time rate $\dot{\mathbf{T}} = {}^{b}\dot{\mathbf{T}}$ of the temperature at time instant $t = {}^{b}t$ in analogy to Eq 9 by the iteration:

$$\dot{\mathbf{T}}_{i+1} = \dot{\mathbf{T}}_i + \mathbf{H}^{T}_i[\dot{\mathbf{Q}} - \mathbf{C}\dot{\mathbf{T}} - \mathbf{K}\mathbf{T} - \mathbf{L}\mathbf{T}]_i \qquad \text{(Eq 18)}$$

The iteration matrix is taken as:

$$\mathbf{H}^{T} = -[\mathbf{G}^{T}]^{-1} \qquad \text{(Eq 19)}$$

and

$$\mathbf{G}^T \leftarrow -\mathbf{C} - \zeta\tau[\mathbf{K} + \mathbf{L}] \quad \text{(Eq 20)}$$

is a convenient approximation to the gradient of the residuum in the brackets in Eq 18 with respect to the iteration variable $\dot{\mathbf{T}}$.

Since the thermal equation (Eq 15) and the mechanical equation (Eq 3) interact via temperature and deformation, they represent a coupled system. The fully algebraic version of this system implies the approximate time integration schemes of Eq 7, 8, and 16 and can be symbolized as:

$$\mathbf{F}^M(\mathbf{V},\dot{\mathbf{T}}) = 0,\ \mathbf{F}^T(\dot{\mathbf{T}},\mathbf{V}) = 0 \quad \text{(Eq 21)}$$

In the numerical computation, the solutions of the above physical subsystems are coupled iteratively. Thereby, the mechanical equations of motion are solved for the velocity at a fixed distribution of temperature and the thermal equations for the temperature rate at a fixed velocity field. The partial solutions can be performed in parallel or in sequence, and the results are exchanged accordingly before a new iteration cycle starts for the coupled problem following Doltsinis (Ref 22, 23).

2.3 *Modifications of the Finite-Element Mesh*

In the following simulations, a Lagrangean approach to the motion of the material has been applied; therefore, the computational mesh follows the material motion. In order to control the severe distortions of the computational mesh inherent in the present approach, a partial or complete regeneration of the discretized mesh has been applied whenever the monitored element shapes exceed a prescribed limit. For quadrangular elements, an aspect ratio of about 2.0 has been found to be a critical threshold value over which remeshing is necessary.

To this end, an automatic mesh generation algorithm (Ref 24) has been modified for activation during the course of the numerical simulation (Ref 25). The original algorithm performs an automatic generation of the finite-element mesh on the basis of geometrical blocks and mean element sizes defined by the user. Its utilization for mesh regeneration during computation is straightforward; the transfer of the numerical solution to the new mesh follows an appropriate interpolation procedure within the finite-element approximation from the previous solution nodal values.

3. Process Parameters and Boundary Conditions

The relevant process parameters for plasma spray are well known; nevertheless, the detailed information needed in our numerical study (for example, particle temperature and velocity inside the flame and particle material properties) are not generally available. This work has used a single set of process parameters, investigated and discussed by Vardelle et al. (Ref 26) for the case of thermal spraying of yttria-stabilized zirconia (8 wt% Y_2O_3). In particular, the following simulations have relied on the measurements of Vardelle et al. on particle size, impact velocity, and in-flight particle surface temperature distributions.

Material data for fused and sprayed zirconia are extremely variable, and only reasonable average values can be usefully deduced from the literature. Viscosity is perhaps the most critical material parameter to assess. The following temperature dependence, deduced by a scaling procedure (Ref 27) based on the experimental measurements of the viscosity of a structurally similar oxide (namely, UO_2) (Ref 28), has been used:

$$\eta = A \exp\left(\frac{4620}{T}\right) \quad \text{(Eq 22)}$$

where T is temperature (K), η is viscosity (Pa · s), and A is a coefficient that remains to be determined for the zirconia material. Table 1 presents the range of process parameters and material data that have been investigated in the following numerical studies.

Another important physical property that depends strongly on spraying conditions is the temperature field inside the particle at impact. Torch characteristics, gas velocity and composition, and particle size and trajectory inside the flame influence heat flows to and from the particle (see, for example, Ref 2). During flight the particle experiences rapid, violent initial heating, followed by cooling at the surface as it exits the flame (Ref 29). Thus, depending on the particular spraying conditions, the final temperature field can be very uniform or unmelted zones can be present inside the particle, with temperature variations on the order of hundreds of degrees. As a first approximation, only completely melted particles with a uniform internal temperature, equal to the average surface temperature measured experimentally (Ref 16), have been considered.

Thermal and mechanical boundary conditions are illustrated in Fig. 2. Thermal boundary conditions comprise heat flow from the droplet to the substrate and to the surrounding gas. The latter is controlled by the emissivity of the material and is a minor contributor to the dissipation of heat during the fast spreading and cooling process. The heat flow to the substrate is the fundamental thermal parameter, as will be confirmed in the present study. It is determined essentially by the interface properties; that is, the thermal conductivity of zirconia and of the substrate material

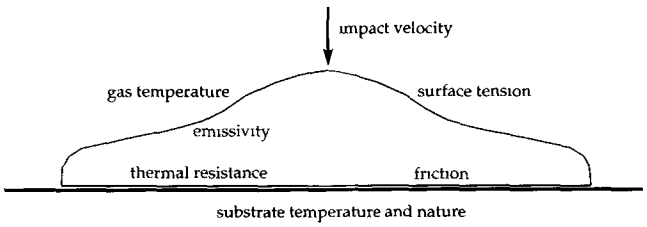

Fig. 2 Thermal and mechanical boundary conditions

Table 1 Process parameters and material data

Process parameters	Unit	Range	Reference value
Particle diameter	μm	20 - 40	20
Particle velocity at impact	m/s	120 - 180	180
Material data			
Density	kg/m^3	5.55×10^3	5.55×10^3
Specific heat	J/kg · K	500 - 1000	500
Thermal conductivity	W/m · K	2	2
Latent heat of solidification	J/K	6.1×10^5	6.1×10^5
Viscosity at 3200 K	kg/ms	4.2 - 42	42

plays a minor role compared to the thermal resistance at the interface.

Mechanical boundary conditions imposed in the model are surface tension and the friction law with the substrate. Surface tension has a negligible effect in retarding the splashing process, compared to viscous dissipation. Friction with the substrate causes the first layers of the particle material either to stick to the substrate or to flow. However, simulations have shown that variation to the friction law only influences deformation of elements close to the contact surface, without influencing the final splat shape. Table 2 presents the range of thermal and mechanical boundary condition parameters investigated in the following numerical studies.

Table 2 Thermal and mechanical boundary conditions

Parameter	Unit	Range	Reference value
Initial particle temperature	K	3200 - 3400	3400
Surrounding gas temperature	K	1200 - 1800	1800
Substrate temperature	K	400 - 1200	1200
Solidus temperature	K	2680 - 2880	2880
Liquidus temperature	K	2700 - 2980	2980
Emissivity	...	0.2 - 0.6	0.4
Convection coefficient	$W/m^2 \cdot K$	$1 \div 5 \times 10^6$	1×10^6
Surface tension	J/m^2	0.5	0.5
Coulomb friction coefficient	...	0.0 ÷ 0.4	0.2

4. Applications

4.1 *Description of the Simulation*

The computational method outlined in Section 2 is available in a nonlinear software program developed at the Institute for Computer Applications (Ref 30). The basic program system has been extended here to comply with the requirements of the impact problem.

A reference simulation run will be presented in detail. It describes a thermomechanical computation of the impact at normal direction of a completely molten spherical particle on a flat, rigid surface. The simulation is followed until the motion of the splat on the surface stops. The thermal calculation is continued to investigate the cooling process until complete solidification of the splat is attained. Axial symmetry is used to decrease the size of the problem.

The mechanical simulation proceeds in steps. The first phase for every impact event always starts with an initial mesh representing a sphere of given radius, velocity, and temperature distribution at the instant of impact with the substrate. Each subsequent simulation phase ends when the element deformation due to mechanical evolution becomes too high to guarantee the quality of the solution The aspect ratio of the quadrangular elements is monitored automatically during the simulation. When it exceeds a prescribed value, the mesh is automatically regenerated following the procedures described in Section 2.3. The calculation is then restarted.

To define the reference case study of the impact, average values of the parameters have been selected from available sets of measurements. These have been performed under controlled conditions on single splatting events of plasma-sprayed zirconia particles at the University of Limoges (Ref 26, 31, 32) (see also Tables 1 and 2).

A typical splat evolution is shown in Fig. 1, which presents a three-dimensional surface rendering of the axisymmetric two-dimensional computation. The remeshing procedure, coupled to an automatic time-step control, allowed complete thermomechanical calculations of the splash in about 10,000 steps, using an axisymmetric mesh of approximately 600 to 1000 elements. Normally, 30 to 45 mesh regenerations were needed, and the necessary processing time on a VAXstation 4000 (Digital Equipment Corporation, Maynard, MA, USA) computer was between 30 and 40 h. The thermal and mechanical evolution is independent of the size of the initial mesh and of the subsequent refinement if a sufficient number of elements is used (>500). The motion of the splashing was considered to be completed when the kinetic energy of the splat fell below 10^{-4} times the initial value. One configuration was followed further and confirmed the validity of the assumption.

4.2 *Results and Sensitivity Studies*

Table 3 summarizes initial data (particle diameter and velocity, and related Reynolds number) and output results (total splat time, time of first appearance of solidification, time of solidification completion, theoretical Madejski's model flattening degree, and computed flattening degree) for nine of the simulations performed. Simulation numbers 7 to 9 refer to results obtained for the same Reynolds number but for different thermal parameters.

The values of ξ obtained from our model are always less than the theoretical previsions of Madejski's model, but are higher than available experimental measurements from Vardelle et al. (Ref 26) (droplets impacting on cold, smooth substrates) and numerical estimates from Yoshida et al. (Ref 15) (data in this case refer to a different material, Al_2O_3). The different data are compared in Fig. 3. In our model, as in the Yoshida calculations, flattening data are reasonably fitted by a relation of Madejski's type (see Ref 2) by using a modified coefficient:

$$\xi = 0.925\, R^{0.2} \qquad \text{(Eq 23)}$$

The experimental curve in Fig. 3 (from Ref 26) is the best fit to numerous data, but the scatter of data (not indicated here) is relevant and encompasses the simulation estimates. The discrepancy between experimental and model values is therefore statistical, in the sense that on average the experimental flattening degrees are lower. This could be interpreted by the assumption that some particles are partially unmelted, whereas the model considers only completely melted particles. Investigations on this matter are under way both experimentally and numerically.

The temporal evolution of ξ and its dependence on mechanical and thermal parameters are shown in Fig. 4. Mechanical parameters such as viscosity, initial velocity, and particle diameter (top of Fig. 4) significantly influence the splashing process. Thermal parameters such as substrate temperature (T_{subs}), initial droplet temperature (T_i), and interface convection coefficient (α_c) (bottom of Fig. 4) are important in the subsequent cooling and solidification phenomena, but have a minor influence on the

Table 3 Results of simulations

n	d, μm	v, m/s	R	t_s(a), μs	t_{ss}(b), μs	t_{es}(c), μs	ξ_M(d)	ξ(e)
1	20	120	317	0.67	0.51	6.50	4.09	3.01
2	20	180	476	0.49	0.50	5.90	4.44	3.24
3	30	150	595	0.45	0.35	12.70	4.64	3.35
4	40	135	714	0.62	0.16	21.00	4.82	3.36
5	40	170	899	0.94	0.18	20.00	5.04	3.50
6	40	180	951	1.08	0.38	13.20	5.10	3.69
7	20	180	476	0.47	0.17	4.30	4.44	3.22
8	30	150	595	0.27	0.27	8.57	4.64	3.25
9	40	170	899	0.14	0.14	13.50	5.04	3.32

(a) t_s, flattening time. (b) t_{ss}, start of solidification. (c) t_{es}, end of solidification. (d) ξ_M, Madejski flattening degree. (e) ξ, model flattening degree

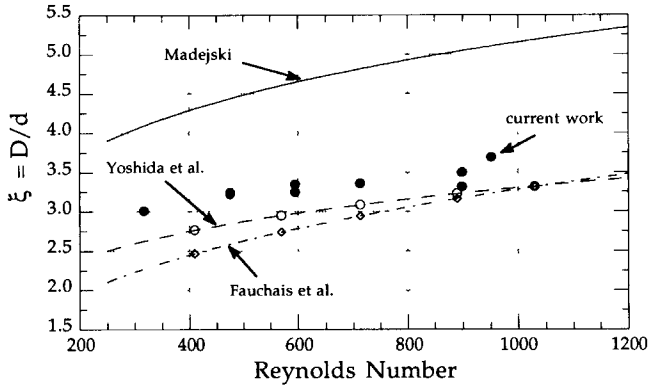

Fig. 3 Flattening degree as a function of Reynolds number. The black points are the results from the current work

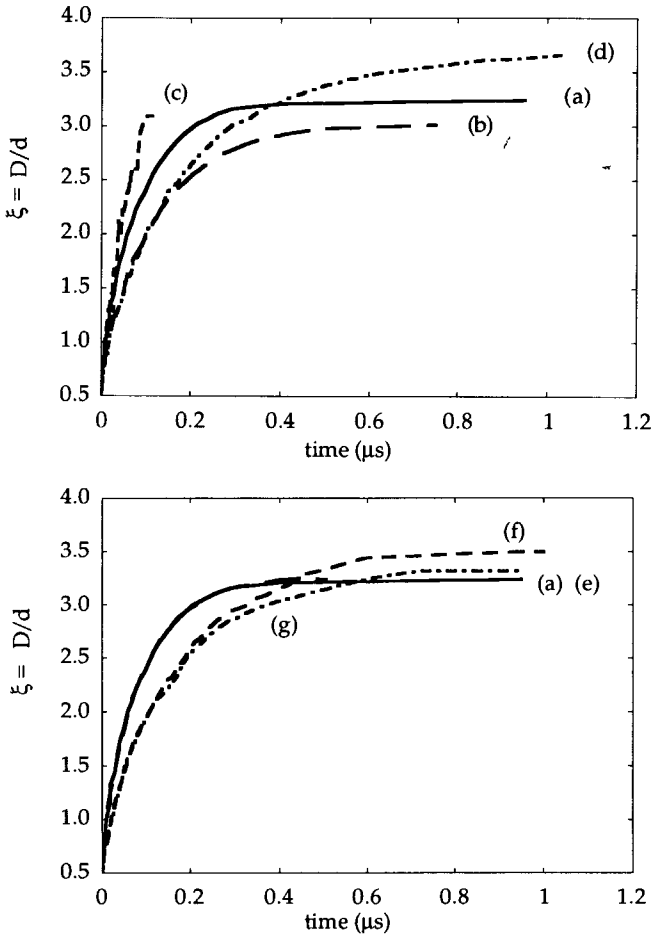

Fig. 4 Flattening degree as a function of time for different cases. Curves a and e follow each other closely. (a) Reference (see Tables 1 and 2); (b) v = 120 m/s; (c) $\eta = 0.97 \exp(4620/T)$ mPa · s; (d) d = 40 μm; (e) T_{sub} = 400 K; (f) d = 40 μm, v = 170 m/s; T_i = 3200, T_{gas} = 1200; (g) like (f), but $\alpha_c = 5 \times 10^6$ W/m^2 · K

spreading process. In fact, for almost all the parameters considered, temporal scales for splashing and solidification are very different (see Table 3); therefore, the two phenomena are in fact decoupled.

The influence of viscosity on the splashing process is relevant. A low viscosity, as expressed in Eq 22 with A = 0.97, corresponds to splats that evolve like a liquid rather than a viscous solid. Figure 5 compares a snapshot of the low-viscosity case (A = 0.97) with a high-viscosity (A = 9.70) model at the same instant. The calculations for the low-viscosity case (curve c in Fig. 4) were interrupted due to the appearance of extensive deformations at the contact surface and high turbulence in the melt (see Fig. 5). For this range of low viscosity, a Eulerian flow approach to the material motion seems more appropriate. In the following simulations, only higher values for the viscosity have been used since the present model is best suited for these cases.

The influence of thermal parameters on flattening degree is moderate, if they are kept within the experimental range for the specific process. Curves a and e in Fig. 4, obtained by varying the substrate temperature from 1200 to 400 K, are essentially superimposed. A change of as much as five times in the interface convection coefficient, α_c (e.g., between curves f and g), causes a variation of only about 7% in ξ. A visual assessment of the influence of thermal parameters on ξ can be made directly in Fig. 3, which plots results for the same Reynolds number but for different thermal parameters.

On the other hand, the same variation of thermal parameters produces overlapping between mechanical evolution and solidification processes. For example, Fig. 6 shows the development of the solidification front inside the splat for cases f and g of Fig. 4. The time instants at which elements undergo solidification is

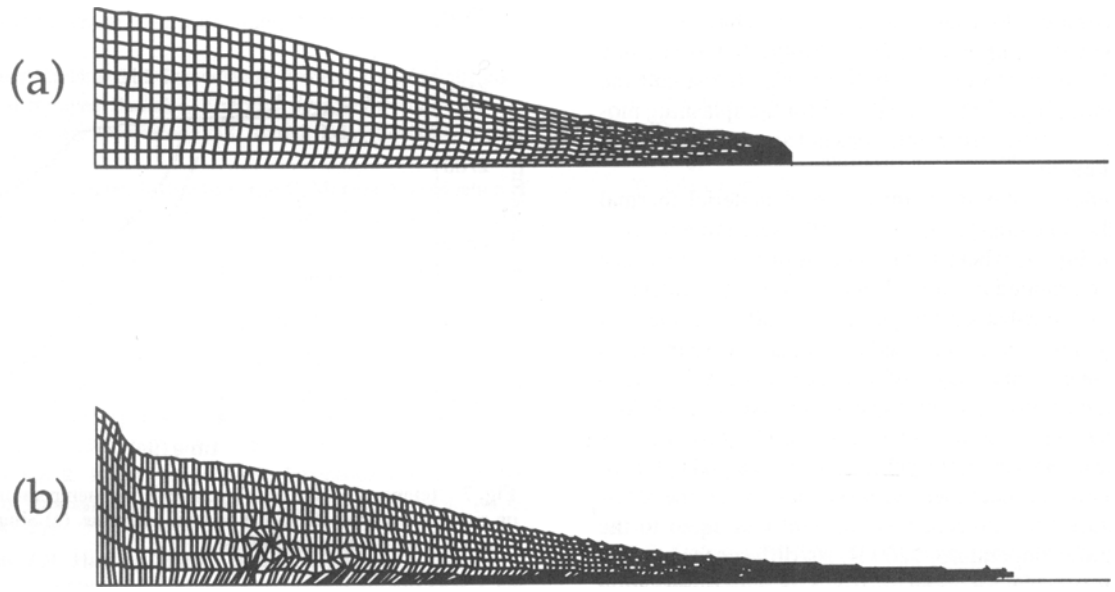

Fig. 5 Deformed mesh after 0.11 μs. (a) $\eta = 0.97 \exp(4620/T)$. (b) $\eta = 9.7 \exp(4620/T)$

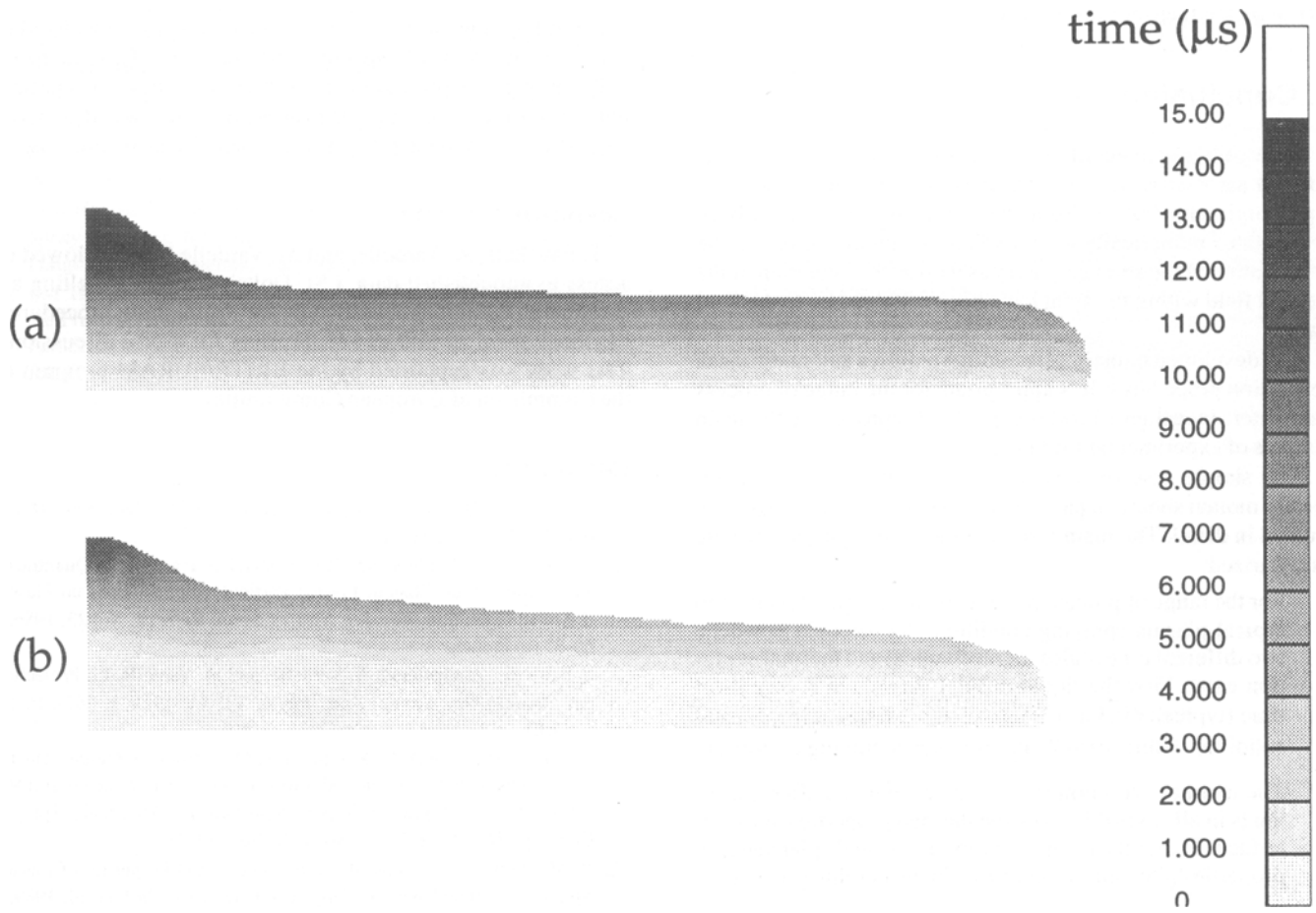

Fig. 6 Solidification inside the splat (time in μs). Note that the splat shapes have been scaled in height (scale 1:2.5) to improve data readability. (a) $\alpha_c = 1 \times 10^6$ W/m$^2 \cdot$ K (curve f in Fig. 4). (b) $\alpha_c = 5 \times 10^6$ W/m$^2 \cdot$ K (curve g in Fig. 4)

shown in the contour plot (note that splat shapes have been exaggerated in height to improve data readability). In the case of a high interface convection coefficient (case g), almost half the splat is solid within 1 μs—the typical time for the splashing motion. However, as noted earlier, this does not significantly affect the flattening degree.

Final evidence of the small influence of material thermal properties in the time range of interest for the spreading process is presented in Fig. 7, where the evolution of average surface temperature is computed for three different substrate model materials for the same substrate temperature, 1200 K. In the first two cases, a cylindrical mesh is used to simulate two substrates (zirconia and steel), while a layer of interface elements is used to impose the same contact thermal resistance (1×10^{-6} m$^2 \cdot$ K/W). In the third case, only a simple convection boundary condition is imposed on the contact area; the value of α_c is set equal to the inverse of the above contact thermal resistance, while the reference temperature for convection is constant and equal to the selected substrate temperature, 1200 K. No differences in cooling behavior are present for about the first 8 μs. This observation indicates that splashing and cooling until solidification are little affected by the nature of the substrate, but rather by the interface thermal resistance. The variation of splat emissivity and thermal conductivity inside the particle had no practical effect on cooling curves and splashing behavior. These observations enforce the assumption that the cooling of the particle is essentially driven by the interface properties.

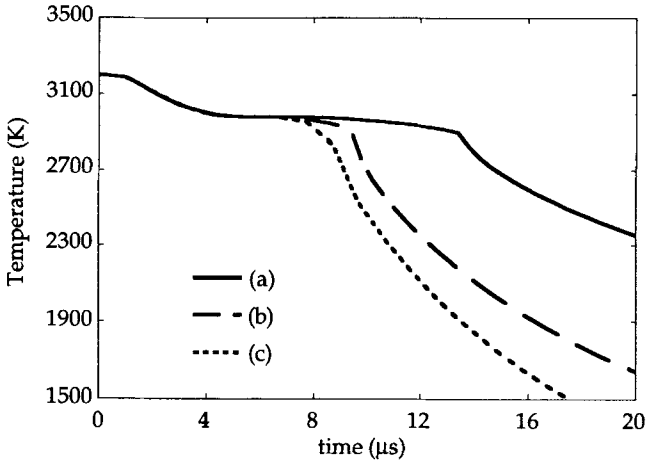

Fig. 7 Temporal evolution of average surface temperature. (a) Splat on zirconia substrate. (b) Splat on steel substrate. (c) Simple convection boundary condition at interface

5. Conclusion

Flow of liquid material, heat transfer, and solidification phenomena associated with the impingement, spreading, and cooling of high-temperature droplets on solid substrates have been investigated numerically within a finite-element approach. The deformation of the splat geometry as well as the evolution of the thermal field within the splat have been followed up to the final state.

The developed numerical technique requires automatic mesh generation procedures. It is appropriate for the range of process parameters investigated and is capable of reproducing the main features of experimental findings.

The simple case of impact at normal direction of a completely molten spherical particle on a flat, rigid surface has been studied in detail. The main results of the investigations are here summarized:

- For the range of process parameters investigated relative to typical plasma spraying conditions for zirconia powders, two different time scales for mechanical and thermal evolution exist. First the liquid droplet spreads in a very short time (typically 0.5 to 1.0 μs), then it continues to cool and solidifies within 10 to 20 μs from the beginning of impact.
- The thermal evolution in the splat during and after splashing is in all cases driven by the thermal properties of the interface. Thermal exchanges with the gas and splat material properties play only a minor role in the cooling process.
- The computed flattening degrees are well below the theoretical previsions of a previous model (Ref 13). The results of the simulations are reasonably fitted for small particles by a relation of Madejski's type (see Ref 2), but using a modified coefficient equal to 0.925.

More experimental validation is necessary to further improve the model. Work is in progress to obtain such information.

With regard to the modeling effort, extensions of the present study will consider partially melted particles. Implementation of a mixed Lagrangean-Eulerian approach is being considered to extend the model for lower-viscosity materials. This extension will complete the present model and allow its possible application within the wide range of process parameters and material properties found in the plasma spray manufacturing process.

Acknowledgments

P. Fauchais, A. Vardelle, and M. Vardelle kindly allowed us access to unpublished data. I.St. Doltsinis and S. Noelting assisted us in the implementation of their remeshing procedures. We thank them as well as J.H. Harding for useful discussions. This work was supported by the BRITE/EURAM program of the Commision of European Communities.

References

1. J.H. Zaat, A Quarter Century of Plasma Spraying, *Ann. Rev. Mater. Sci.*, Vol 13, 1983, p 9-42
2. A. Vardelle, M. Vardelle, and P. Fauchais, Les Transfers de Quantité de Mouvement et de Chaleur Plasma Particules Solides dans un Plasma d'Arc en Estinction, *Rev. Int. Hautes Temp. Refract.*, Vol 23, 1986, p 69-85 (in French)
3. P. Fauchais, A. Grimaud, A. Vardelle, and M. Vardelle, La Projection par Plasma: Une Revue, *Ann. Phys.*, Vol 14, 1989, p 261-310 (in French)
4. D.S. Rickerby, G. Eckold, K.T. Scott, and I.M. Buckley-Golder, The Interrelationship between Internal Stress, Processing Parameters and Microstructure of Physically Vapor Deposited and Thermally Sprayed Coatings, *Thin Solid Films*, Vol 154, 1987, p 125-141
5. R. McPherson, A Review of Microstructure and Properties of Plasma Sprayed Ceramic Coatings, *Surf. Coat. Technol.*, Vol 39-40, 1989, p 173-181
6. J. Mishin, M. Vardelle, J. Lesinski, and P. Fauchais, Two Colour Pyrometer for the Statistical Measurement of Particulate Surface Tem-

perature under Thermal Plasma Conditions, *J. Phys. E*, Vol E20, 1987, p 620

7. C. Moreau, P. Cielo, and M. Lamontagne, Flattening and Solidification of Thermal Sprayed Particles, *Thermal Spray: International Advances in Coatings Technology*, C.C. Berndt, Ed., ASM International, 1992, p 761-766
8. S. Fantassi, M. Vardelle, P. Fauchais, and C. Moreau, Investigation of the Splat Formation versus Different Particulate Temperatures and Velocities prior to Impact, *Thermal Spray: International Advances in Coatings Technology*, C.C. Berndt, Ed., ASM International, 1992, p 755-760
9. A.M. Worthington, *A Study of Splashes*, MacMillan, 1963
10. G. Trapaga, E.F. Matthys, J.J. Valencia, and J. Szekely, Fluid Flow, Heat Transfer, and Solidification of Molten Metal Droplets Impinging on Substrates: Comparison of Numerical and Experimental Results, *Metall. Trans. B*, Vol 23B, 1992, p 701-718
11. O. Knotek and R. Elsing, Monte Carlo Simulation of the Lamellar Structure of Thermally Sprayed Coatings, *Surf. Coat. Technol.*, Vol 32, 1987, p 261-271
12. S. Cirolini, J.H. Harding, and G. Jacucci, Computer Simulation of Plasma-Sprayed Coatings: I. Coating Deposition Model, *Surf. Coat. Technol.*, Vol 48, 1991, p 137-145
13. J. Madejski, Solidification of Droplets on a Cold Surface, *J. Heat Mass Transfer*, Vol 19, 1976, p 1009-1013
14. G. Trapaga and J. Szekely, Mathematical Modeling of the Isothermal Impingement of Liquid Droplets in Spraying Processes, *Metall. Trans. B*, Vol 22B, 1991, p 901-914
15. T. Yoshida, T. Okada, H. Hideki, and H. Kumaoka, Integrated Fabrication Process for Solid Oxide Fuel Cells using Novel Plasma Spraying, *Plasma Sources Sci. Technol.*, Vol 1, 1992, p 195-201
16. S. Fantassi, M. Vardelle, A. Vardelle, and P. Fauchais, Influence of the Velocity of Plasma Sprayed Particles on the Splat Formation, *Thermal Spray Coatings: Research, Design and Applications*, C.C. Berndt, Ed., ASM International, 1993, p 1-6
17. J.M. Houben, Future Developments in Thermal Spraying, *Thermal Spray Coatings: New Materials, Processes and Applications*, F.N. Longo, Ed., ASM International, 1985, p 1-19
18. J.M. Houben, "Relation of the Adhesion of Plasma Sprayed Coatings to the Process Parameters Size, Velocity and Heat Content of the Spray Particles," Ph.D. thesis, Technische Universiteit, Eindhoven, The Netherlands, 1988
19. M. Bertagnolli, M. Marchese, G. Jacucci, I.St. Doltsinis, and S. Noelting, Finite Element Thermomechanical Simulation of Droplets Impacting on a Rigid Substrate, *Materials and Design Technology 1994*, Vol 62, T.J. Kozik, Ed., American Society of Mechanical Engineers, 1994, p 199-210
20. J. Argyris, I.St. Doltsinis, H. Fischer, and H. Wüstenberg, Τα πάντα ρεῖ, *Computer Meth. Appl. Mech. Eng.*, Vol 51, 1985, p 289-362
21. I.St. Doltsinis, J. Luginsland, and S. Nölting, Some Developments in the Numerical Simulation of Metal Forming Processes, *Eng. Comput.*, Vol 4, 1987, p 266-280
22. I.St. Doltsinis, Aspects of Modelling and Computation in the Analysis of Metal Forming, *Eng. Comput.*, Vol 7, 1990, p 2-20
23. I.St. Doltsinis, Coupled Field Problems—Solution Techniques for Sequential and Parallel Processing, *Solving Large Scale Problems in Mechanics*, M. Papadrakakis, Ed., John Wiley & Sons, 1993
24. I.St. Doltsinis and S. Nölting, Generation and Decomposition of Finite Element Models for Parallel Computations, *Comput. Sys. Eng.*, Vol 2, 1992, p 427-449
25. I.St. Doltsinis, M. Eggers, S. Nölting, and G. Nötzel, "Finite Element Modelling of Ceramic Thermal Barrier Coatings to Extend the Operating Range of Heat Engine Components," 1st Internal Work Report, ICA-Stuttgart, 1992
26. M. Vardelle, A. Vardelle, P. Fauchais, and C. Moreau, Pyrometer System for Monitoring the Particle Impact on a Substrate during a Plasma Spray Process, *Meas. Sci. Technol.*, Vol 5, 1994, p 205-212
27. J.H. Harding, private communication, AEA Technology, Didcot, U.K., 1993
28. J.L. Fink, M.G. Chasanov, and L. Leibowitz, "Transport Properties of Uranium Dioxide," ANL-CEN-RSD-80-4, Argonne National Laboratory Report, 1981
29. R. Westhoff, G. Trapaga, and J. Szekely, Plasma-Particle Interactions in Plasma Spraying Systems, *Metall. Trans. B*, Vol 23B, 1992, p 683-693
30. H. Wüstemberg, "FEPS 3.3 Finite Element Programming System: User's Guide," ICA Report No. 21, Stuttgart, 1986; "FEPS 3.3: Elements Library," ICA Report No. 22, Stuttgart, 1986
31. "Modeling and Characterization of the Manufacturing Process of Ceramic Thermal Barrier Coatings," BRITE/EURAM Project No. BREU-0418, Second periodical report, CEC, Brussels, 1992
32. "Modeling and Characterization of the Manufacturing Process of Ceramic Thermal Barrier Coatings," BRITE/EURAM Project No. BREU-0418, Third periodical report, CEC, Brussels, 1993